Rotor Performance of a UH-60 Rotor System in the NASA Ames 80- by 120-Foot Wind Tunnel

Patrick M. Shinoda
Army/NASA Rotorcraft Division
US Army Aeroflightdynamics Directorate (AMCOM)
pshinoda@mail.arc.nasa.gov

Hyeonsoo Yeo
Raytheon ITSS
hsyeo@mail.arc.nasa.gov

Thomas R. Norman
Army/NASA Rotorcraft Division
tnorman@mail.arc.nasa.gov

NASA Ames Research Center
Moffett Field, California

ABTRACT

A full-scale four-bladed UH-60 rotor system was tested in the NASA Ames 80- by 120-Foot Wind Tunnel. A quality data set at low forward speed, 0 to 80 knots, has been obtained to support future rotor developments and analysis improvements. To evaluate the NASA Ames 80- by 120-Foot Wind Tunnel as a hover testing facility, rotor performance data were compared with predictions, UH-60 aircraft flight test data, and UH-60 model-scale data from other test facilities. Results indicate that valid hover data for this size rotor can be obtained from this facility at low to medium thrust conditions. Comparisons with flight test and model-scale data demonstrate the variability between existing data sets. Predictions show good agreement with full-scale data. To evaluate the analytical modeling in the 0 to 80 knot speed range, forward flight rotor performance data were acquired and compared with predictions. Comparisons were also made with existing model-scale and flight test data. Power calculations show fair to good agreement with full-scale wind tunnel data at advance ratios between 0.10 to 0.19 and poor agreement at advance ratios below 0.10. Comparisons with flight test and model-scale data show good agreement at all advance ratios tested. Propulsive force calculations show good correlation with full-scale wind tunnel data at advance ratios of 0.10 to 0.19.

Presented at the American Helicopter Society 58th Annual Forum, Montreal, Canada. June 11-13, 2002.

NOTATION

A	=	rotor disk area, πR^2, ft^2
b	=	number of rotor blades
c	=	airfoil chord length, ft
c_s	=	speed of sound, ft/s
C_{LR}/σ	=	rotor wind-axis lift coefficient divided by rotor solidity, positive up, $L_R/\rho(\Omega R)^2 S_R$
C_P/σ	=	rotor power coefficient divided by rotor solidity, $P/\rho(\Omega R)^3 S_R$
C_T/σ	=	rotor thrust coefficient divided by rotor solidity, positive up, $T/\rho(\Omega R)^2 S_R$
C_{XR}/σ	=	rotor wind-axis propulsive coefficient divided by rotor solidity, positive forward, $- D_R/\rho(\Omega R)^2 S_R$
C_W/σ	=	weight coefficient divided by rotor solidity, positive up, $GW/A\rho(\Omega R)^2$
DL	=	Download force on the fuselage, lb
D_R	=	rotor wind-axis drag, positive downstream, lb
F_M	=	Figure of merit, $C_T^{3/2}/C_P\sqrt{2}$

F_{tether} = tether force, lb

GW = aircraft gross weight, lb

L_R = rotor wind-axis lift, positive up, lb

M_{TIP} = rotor tip Mach number, $\Omega R/c_s$

P = rotor shaft power, Torque * Ω, ft-lb/s

r = rotor blade radial location, ft

R = rotor radius, ft

S_R = rotor blade area, bcR, ft^2

T = rotor thrust, lb

V_∞ = free stream velocity, ft/s

Z = rotor hub height from the ground or test section floor

α_S = rotor shaft angle, positive aft of vertical, deg

μ = advance ratio, $V_\infty/\Omega R$

ρ = free-stream air density, $slug/ft^3$

σ = rotor solidity, $bc/\pi R$

Ω = rotor rotational speed, rad/s

INTRODUCTION

Wind tunnel testing has been extensively used in the development and improvement of rotorcraft designs in addition to providing databases for refinement of theoretical models. To date, however, there have been only a few tests that have provided data in the low speed flight regime (below 60 knots) that are suitable for the validation of prediction codes. One such test was the S-76 full-scale test (Ref. 1) in the NASA Ames 80- by 120-Foot Wind Tunnel (80 x 120).

The Sikorsky Aircraft UH-60 is one of the more thoroughly tested rotor systems, having undergone extensive flight and model-scale wind tunnel testing. This testing has included hover and forward flight performance tests conducted by the U.S. Army Aviation Engineering Flight Activity (AEFA) at Edwards AFB (Refs. 2-6) and tests of a highly-instrumented rotor at the U.S. Army Aeroflightdynamics Directorate and NASA Ames Research Center (Refs. 7-16). Model-scale testing has included two hover tests performed at the Sikorsky Model Hover Test Facility at Stratford, Connecticut (Refs. 17-19), and a follow-on wind tunnel test conducted at the Duits-Nederlandse Windtunnel (DNW) in the Netherlands (Refs. 20-22).

To expand the existing UH-60 database and to investigate rotor performance and loads in the low speed flight regime, a full-scale UH-60 rotor test (Ref. 23) has been conducted in the 80 x 120. In this paper, the results from this test program will be compared with flight test and model-scale test data, and with predictions to 1) evaluate the capability of the 80 x 120 as a hover facility, 2) evaluate analytical modeling capabilities in the 0-80 knot speed range and 3) characterize the adequacy or limitations of UH-60 model-scale, full-scale, and flight test data.

This paper presents a brief description of the current wind tunnel test as well as the analytical model and previous UH-60 tests that will be used in the discussion. Hover and forward flight rotor performance results are discussed and compared with flight test data, model-scale wind tunnel test data, and analytical calculations. Finally, conclusions of the research are presented.

DESCRIPTION OF THE TEST

The following section provides a brief description of the test, including the model, the primary measurement system and the test conditions. A more detailed description of the test and the facility can be found in Ref. 23.

Model

The experiment was conducted in the NASA Ames 80- by 120-Foot Wind Tunnel using a production Sikorsky Aircraft UH-60A rotor system mounted on NASA's Large Rotor Test Apparatus (LRTA). Figure 1 shows the model installed in the wind tunnel.

The rotor system, including the hub, spindles, blades, and swashplate, is identical to the one used on the production aircraft. The rotor is four-bladed with coincident flap and lag articulation provided at the blade root by elastomeric bearings. The elastomeric bearing, through the rotor spindle, also allows blade pitch motion. No bifilars were installed in the test program. Pertinent UH-60A rotor parameters are listed in Table 1.

The LRTA test stand was designed for testing large-scale helicopter rotors and tilt rotors in the NASA Ames National Full-Scale Aerodynamics Complex (including the 80 x 120). The test stand houses two electric drive motors, a transmission, rotor balance, self-contained lubrication system, and a primary and dynamic control system. The

LRTA is capable of testing rotors up to a 52,000 lb thrust and 6,000 Hp as well as measuring six-components of both steady and dynamic rotor hub loads. The primary controls consist of three electrical-mechanical actuators that provide conventional collective and cyclic pitch control. A hydraulic-based dynamic control system is integrated into the primary control system and can excite the non-rotating swashplate from 0 to approximately 25 Hz. The LRTA fairing (a symmetrical body of revolution 40-ft in length and 8.33-ft in diameter) is mounted independently of the LRTA chassis frame on load cells and provides fuselage forces (lift, drag, side force) and moments (pitch, roll, yaw).

The LRTA was mounted in the wind tunnel on a three-strut (two main struts and one tail strut) support system placing the rotor hub nominally 40-ft above the wind tunnel floor. The model angle-of-attack was varied by changing the height of the gimbaled tail strut.

Primary Measurements

The performance measurements discussed in this paper were obtained from the LRTA five-component balance and flex coupling. The balance measures rotor normal, axial and side forces, together with the rotor pitching and rolling moments. The instrumented flex coupling measures rotor torque and residual power-train normal force. Both rotor balance and flex coupling were designed to measure static and dynamic loads. For this program, however, the measurement systems were only calibrated statically. Table 2 lists the general balance capabilities and Table 3 the accuracy of the system. Detailed information on the balance, including calibration procedures, can be found in Ref. 24.

Test Conditions

Performance data were acquired in hover and forward flight over a range of thrust, speed, and shaft angle including 1) speed sweeps at specific thrusts and rotor shaft angles-of-attack, and 2) thrust sweeps at specific tunnel velocities and rotor shaft angles-of-attack. The full range of test conditions is shown in Tables 4, 5 and 6. Possible effects of outside winds were reduced by performing low speed testing when the ambient wind speeds were less than 5 knots and the non-fan-driven air speed through the test section was less than 4 knots. All data presented in this paper were acquired with the first harmonic flapping trimmed to near zero (± 0.4 deg) with no wall corrections applied.

DESCRIPTION OF PREVIOUS TESTS

Rotor performance data from two flight test programs and three model-scale wind tunnel programs are presented in this paper. This section provides a summary of these tests.

The first set of flight test programs considered (Refs. 2-6) was conducted by AEFA and consisted of a series of flight tests on different UH-60A aircraft. The data used in this paper are the hover data from the 1st Year production UH-60A aircraft and the 12th Year production aircraft. The primary difference between these aircraft was the installation of fairings for the Extended Stores Support System (ESSS) that became the standard configuration on all UH-60's from the 6th Year production aircraft to the present. In both AEFA tests, the aircraft gross weight (GW) was determined using the tethered hover technique and the only power measurement was total engine power. Hover data were acquired at a rotor hub height to rotor radius ratio (Z/R) of 3.73 with winds under 3 knots.

The second flight test program was the UH-60A Airloads Program (Refs. 7-16) conducted by Army/NASA. Data from both the hover and forward flight portions of this test program are used in this paper. The UH-60A aircraft used during this program was highly instrumented and included both shaft and total engine power measurements. The hover data were (mostly) housekeeping points (same Z/R as the AEFA tests) but there was no control on winds nor was the tethered hover technique used. This resulted in significantly greater scatter than the AEFA test hover data. Forward flight comparisons are made using level-flight data acquired at $C_W/\sigma = 0.08$ and 0.09.

The first two small-scale programs were hover tests conducted at the Sikorsky Model Hover Test Facility. The first test (Ref. 17) used a 1/5.97-scale model of the UH-60 helicopter (including fuselage and tail rotor) with rotor blades 8.98 feet in diameter. The blades were dynamically scaled and had representative coning angles, with a slightly larger blade solidity of 0.08504 compared to 0.0826 of the standard rotor. Hover testing was conducted both with and without the fuselage to measure isolated hover performance and fuselage download in and out of ground effect. The hover performance data presented in this paper are from the isolated rotor test with $M_{TIP} = 0.650$. Fuselage download measurements are used to evaluate ground effect in the 80 x 120.

The second hover test (Refs. 18,19) used a 1/5.73-scale model UH-60 rotor system with rotor blades 9.4 feet in diameter. The blades matched the geometry of the full-scale rotor, with the exception of no trim tabs, and included 176 blade-mounted pressure transducers. The addition of these pressure transducers increased the blade weight by 30 percent, decreased some modal frequencies by as much as 10 percent, and reduced blade coning by one degree in hover. The data presented in this paper are for M_{TIP} values ranging from 0.60 to 0.70.

The third small-scale program was conducted at the DNW and was used for hover and forward flight comparisons

(Refs. 20-22). This program used the same model rotor as in the second hover test above and was conducted in the DNW open jet test section. All forward flight data were corrected for wind tunnel wall effects using Heyson's method (Ref. 25). The data presented in this paper are for M_{TIP} = 0.629 - 0.700.

DESCRIPTION OF ANALYTICAL MODEL

Rotor performance calculations were performed using the comprehensive rotorcraft analysis CAMRAD II. This model has been used previously for performance correlation with UH-60 flight test data and has shown generally good results (Ref. 26). For the comparisons in this paper, the UH-60A was modeled as an isolated rotor. The rotor was modeled as a flexible blade with nonlinear finite elements. The aerodynamic model included a wake analysis to calculate the rotor non-uniform induced-velocities using free wake geometry. This rotor wake analysis used second-order lifting line theory, with the general free wake geometry calculation. A single-peak model was used for the performance calculations.

The trim solution for the hover condition solved for the collective angle to achieve the specified thrust level. The tip vortex formation process for hover (initial radial contraction and initial vertical convection) was calibrated using measured wake geometry (Ref. 27). The trim solution for forward flight solved for the controls to achieve the specified thrust level and zero 1/rev longitudinal and lateral flapping angles.

RESULTS AND DISCUSSION

In the following sections, hover and forward flight performance measurements are presented and compared with flight test data, model-scale test data, and CAMRAD II calculations.

Hover Performance

The primary objective of the hover testing was to evaluate the capability of the 80 x 120 as a hover test facility. To accomplish this objective, data were acquired over a range of thrust values at several shaft angles (Table 4). In the sections below, these data are presented and compared with other experimental data and predictions.

Wind Tunnel Test Results

Figure 2 shows hover figure of merit at four rotor shaft angles ranging from –15° to +7.5° with thrust levels up to C_T/σ = 0.07. (The thrust range was limited by facility power limitations at the time the hover data were acquired.) The data indicate a performance effect (up to ΔF_M = 0.05) due to shaft angle. The maximum figure of merit was obtained at 0 degrees shaft angle and the minimum was obtained at –7.5 degrees shaft angle throughout the thrust range. This can be seen more clearly in Fig. 3, with the data plotted as a function of shaft angle at constant C_T/σ.

It was expected that the wind tunnel walls would have some effect on the hover performance measurements, especially at 0 degrees shaft angle. It was hoped that at higher shaft angles (plus or minus) the effect of the walls would be reduced, with the rotor wake convected down the tunnel rather than recirculated. This would result in hover performance measurements reaching a minimum as shaft angle was increased. The results shown in Figs. 2 and 3 do indicate a possible ground effect at 0 degrees shaft angle, with increased hover performance at this condition. However, the effect of shaft angle was not as expected, with hover performance improving as the shaft angle was decreased from -7.5 to -15 deg.

To further investigate the possibility of ground effect, the download on the LRTA fuselage was compared with model-scale test results from Ref. 17. As shown in Fig. 4, the LRTA results are consistent with model-scale UH-60 data when the fuselage and rotor were out of ground effect (OGE). Although the fuselage shapes were different, the similarity in results suggest that the LRTA may also have been out of ground effect for α_s = 0 deg.

Comparison with Flight Test Data

Figures 5 and 6 compare measured hover performance data from the 80 x 120, the AEFA 1st Year and 12th Year production aircraft tests, and the Airloads Program. For these comparisons, no corrections to the flight test data were made. Figure 5 shows rotor power and Fig. 6 shows figure of merit as a function of rotor thrust. Both figures indicate higher power required in the flight tests ($\Delta C_P/\sigma$ = 0.0005 – 0.0009 or ΔF_M = 0.05 – 0.09). This was expected since total engine power (as measured in the flight tests) is not equivalent to rotor shaft power (as measured in the wind tunnel). The UH-60A Airloads data agree better with the AEFA 12th Year production aircraft data than the 1st Year data, but show a great deal of scatter. This scatter is due in part to variable wind conditions during testing (Ref. 28). Curiously, the 1st and 12th Year data vary from each other by 0.02 to 0.04 in figure of merit. The exact cause for these differences are not known, although some possibilities are discussed in Ref. 16.

To better compare with 80 x 120 hover wind tunnel data, two corrections were applied to the flight test data. The first was a correction to rotor thrust to account for fuselage

download and the second was a correction to total engine power to estimate rotor shaft power. For the first correction, an estimate of fuselage download (DL) was made using data from the model-scale test (Ref. 17). Figure 4 shows the UH-60 fuselage download as a function of rotor thrust. The gross weight values from the AEFA tests were then corrected using the following equation

$$C_T/\sigma = \frac{C_W/\sigma}{(1-k)} \qquad (1)$$

where k = DL/T was obtained from Fig. 4. These corrections were applied to data from all three flight tests. For the second correction, data from the Airloads Program was used to correct the power measurements from the two AEFA tests. In particular, the average ratio of shaft power to engine power was determined from Airloads hover data. This ratio (0.87) was then applied to the AEFA engine data to provide an estimate of rotor shaft power.

Figure 7 compares the 80 x 120 figure of merit data with corrected data from the AEFA and Airloads tests. The AEFA data, particularly the 12th Year data, show reasonable agreement with the wind tunnel results except at the two highest wind tunnel thrust conditions. In this overlap zone, the 80 x 120 data are low by 0.02 to 0.03 in figure of merit. The Airloads data also show reasonable agreement, although definitive conclusions are not possible due to scatter in the data.

Comparison with Model-Scale Data

Figures 8 and 9 compare measured hover performance data from the 80 x 120 with three sets of model data. Figure 8 shows rotor power as a function of rotor thrust and includes 80 x 120 data at all shaft angles and small-scale data at multiple tip Mach numbers. Figure 9 shows figure of merit as a function of rotor thrust and includes 80 x120 data at a single shaft angle (0 deg) and model data at one tip Mach number.

Both figures indicate reasonable agreement between full-scale and model-scale results, with less power required in model-scale. Reference 17 data match well with the 80 x 120 data except at the two highest 80 x 120 thrust points (ΔF_M = 0.02-0.03). References 18 and 19 data set has the same shape as the 80 x 120 data but is offset by ΔF_M = 0.015 throughout the thrust range. The DNW data match the 80 x 120 data below C_T/σ of 0.05 but diverges from the 80 x 120 data at higher thrust conditions. Differences between the three model-scale tests at high thrust can be seen in Fig. 9 (up to ΔF_M = 0.02-0.05).

In hopes of improving the correlation, the effects of model-scale on hover performance were estimated following the methods of Keys et al (Ref. 29). Assuming a model-scale ratio of 1/5.73 and a full-scale rotor drag coefficient of 0.01, the method suggests that model figure of merit should be approximately 0.03 to 0.04 below the full-scale data. The data in Fig. 9, however, indicate that the opposite is true.

Comparison with Flight Test and Model-Scale Data

Data from all the flight and model-scale tests are compared to 80 x 120 data in Fig. 10. The flight test data have been corrected for power and thrust as discussed previously.

The results show fair correlation of the 80 x 120 data with data from the 12th Year production aircraft, the Airloads Program, and the two Sikorsky hover tests. Data from both the 1st Year production aircraft and the DNW test are significantly higher than the other test data. These results indicate that the 80 x 120 can be used as a hover facility for this size rotor, at least at lower thrust conditions ($C_T/\sigma \leq$ 0.07). Definitive conclusions at higher thrust conditions are not possible, however.

Comparison with Predictions

Figure of merit predictions using CAMRAD II are compared with 80 x 120 and AEFA flight test data in Fig. 11. The predictions match well with the 80 x 120 data at low thrust, but are higher than the data at high thrust. The predictions fall between the flight test results, over predicting the 12th Year data (up to ΔF_M = 0.02) and under predicting the 1st Year data (up to ΔF_M = 0.03).

Rotor Performance at Low Speed

The primary objective of the forward-flight testing was to acquire low-speed performance data for comparison with and validation of analyses. To accomplish this objective, data were acquired over a range of advance ratios, shaft angles, and thrust levels (Tables 5 and 6). In the sections below, these data are presented and compared with other experimental data and predictions.

Wind Tunnel Test Results

Speed sweep data are presented in Figs. 12-13 and thrust sweep data are presented in Figs. 14-21. In general, the data show smooth trends and are consistent with previously acquired low-speed data (Ref. 1). It is anticipated that these data will provide an excellent validation set for analytical development.

Figures 12 and 13 show the effect of advance ratio on rotor power at specific thrusts and shaft angles. As expected, power increased with decreasing advance ratio and increasing thrust for all conditions tested. For the shaft angle variation, power increased as the rotor was tilted forward ($C_T/\sigma = 0.09$).

Figures 14-17 show the effect of rotor lift on rotor power at specific advance ratios and shaft angles. As expected, power increased with increasing lift and decreasing shaft angle. The effect of advance ratio can be seen in the shape and spacing of the curves, with larger power differences between shaft angles at the higher advance ratios.

Figures 18-21 show the effect of rotor lift on propulsive force at specific advance ratios and shaft angles. For negative shaft angles, propulsive force increased linearly with increasing lift and for positive shaft angles, propulsive force decreased. There was no significant effect due to advance ratio.

Comparison with Flight Test Data

To help validate the 80 x 120 data, comparisons were made with data from the UH-60A Airloads Program. To match conditions between experiments, the measured tip-path-plane angle and weight coefficient from flight were used to interpolate 80 x 120 data (assuming $C_W/\sigma = C_{LR}/\sigma$ and shaft angle is equivalent to tip-path-plane angle). Figure 22 is an example of the 80 x 120 data used for interpolation, showing power as a function of rotor shaft angle and μ for a constant lift.

The final comparisons for two weight coefficients, C_W/σ = 0.08 and 0.09, are shown in Figs. 23 and 24. (Curve fits of the wind tunnel data are also shown to indicate the range of interpolation.) In Fig. 23, speed sweep data from the flight test are compared with interpolated 80 x 120 data for C_W/σ = 0.08. The data match well (within $\Delta C_P/\sigma = 0.0002$) above an advance ratio of 0.09, but do not match well below this speed (up to $\Delta C_P/\sigma = 0.0015$). Similar results can be seen in Fig. 24 for C_W/σ= 0.09. The differences at low advance ratios have a number of possible causes. These include 80 x 120 facility effects (re-circulation), flight test external conditions (wind direction, wind turbulence) and flight test low-speed measurement errors (flight speed, aircraft attitude, flight control conditions). The exact cause of these differences is not known.

To show all the power results for the flight and wind tunnel test on one graph, Fig. 25 was generated. The graph compares the Airload Program power with the interpolated 80 x 120 power at all related thrust and tip-path-plane angle conditions. The straight line represents the power values if the data from the two test programs were perfectly correlated. As can be seen, the data deviates from the line at higher power, corresponding to advance ratio conditions less than 0.09.

Comparison with Model-Scale Data

Comparisons were also made with data from the DNW model-scale test. Since test conditions were not identical, the corrected rotor tip path plane angle and corrected rotor lift coefficient from the DNW test were used to interpolate 80 x 120 data. There was no compensation for differences in tip Mach number. The final comparisons for three different advance ratios (μ = 0.10, 0.15, 0.175) are shown in Figs. 26-28.

The data match well (within $\Delta C_P/\sigma = 0.0002$) throughout the thrust range for all advance ratios compared. One interesting observation is that for the two higher advance ratios (Figs. 27 and 28), the DNW data show a slightly lower power requirement than the 80 x 120 data at negative angles and a slightly higher power requirement at positive angles.

To show all the power results for the two wind tunnel tests on one graph, Fig. 29 was generated. The graph compares the DNW power with the interpolated 80 x 120 power at all related thrust and tip-path-plane angle conditions. Once again, the straight line represents the power values if the data from the two test programs were perfectly correlated. In this case, the data match well at all power levels.

The effects of model scale on forward flight performance were estimated using the methods of Keys et al (Ref. 29). Using the same assumptions as discussed in the hover section of this paper, the DNW power should be approximately $\Delta C_P/\sigma$ = 0.0003 higher than the 80 x 120 results. Figure 29 shows an increase in power for the small-scale rotor at lower power levels but is not consistent at the higher levels.

Comparison with Predictions

To evaluate the capability of predicting low-speed performance, CAMRAD II calculations were performed for all 80 x 120 speed sweep and thrust sweep conditions. Figure 30 is an example comparison for speed sweeps at one shaft angle. The predictions differ from the measurements at all thrust conditions, overpredicting power at $\mu > 0.10$ (up to $\Delta C_P/\sigma = 0.0004$) and underpredicting power at $\mu < 0.10$ (up to $\Delta C_P/\sigma = 0.0006$).

Comparisons of CAMRAD II calculations with thrust sweep data are shown in Figs. 31-34 for four advance ratios (μ = 0.10, 0.15, 0.175, and 0.19). Figure 31 shows rotor power as

a function of lift at a fixed advance ratio of 0.10. CAMRAD II matches or underpredicts the 80 x 120 power data by $\Delta C_P/\sigma$ of 0.0002 for shaft angles of –10 deg, -5 deg, and 0 deg. At the shaft angle of +5 deg, CAMRAD II matches the 80 x 120 data throughout the lift range. As shaft angle is increased to +10 deg, CAMRAD II matches the 80 x 120 data at the low thrust condition but overpredicts power by $\Delta C_P/\sigma$ of 0.0003 at the high thrust condition.

At $\mu = 0.15$ (Fig. 32), the calculated power now matches the 80 x 120 data at shaft angles of –10 deg and –5 deg. But at shaft angles of 0 deg and +5 deg, CAMRAD II overpredicts power by $\Delta C_P/\sigma$ of 0.0002 at low thrusts and gradually increases the overprediction to $\Delta C_P/\sigma$ of 0.0005 at the highest thrust condition. These same trends can be seen at the two higher advance ratios (Figs. 33 and 34). The general result is that CAMRAD II overpredicts the required power and that this over prediction increases with increasing lift, shaft angle and advance ratio.

The effects of rotor shaft angle and thrust on rotor propulsive force for advance ratios of 0.10 are shown in Fig. 35. CAMRAD II calculations show a small underprediction of 80 x 120 propulsive force, $\Delta C_{XR}/\sigma = 0.001$, for all shaft angles except for -10 deg where it matches 80 x 120 data. This pattern is consistent at all other advance ratios tested ($\mu = 0.15, 0.175, 0.190$).

These comparisons show that although CAMRAD II calculations provide fair agreement with 80 x 120 power measurements, additional improvements are needed, especially at low speeds.

CONCLUSIONS

A quality data set at low forward speed has been obtained to support future rotor developments and theory improvements. Rotor performance results from the UH-60 test in the 80- by 120-Foot Wind Tunnel have been compared with calculations and other test results. The study has resulted in the following conclusions:

Hover Performance Data

1. The 80 x 120 data indicate a performance effect (up to $\Delta F_M = 0.05$) due to shaft angle with the maximum figure of merit obtained at 0 degrees shaft angle. The 80 x120 can be a useful hover facility at low thrust conditions for this size rotor ($C_T/\sigma \leq 0.07$).

2. The 80 x 120 data show reasonable agreement ($\Delta F_M = 0.02$) with the AEFA flight test data, particularly the 12th Year data, except at the two highest wind tunnel thrust conditions. The Airloads Program data also show reasonable agreement, although definitive conclusions are not possible due to scatter in the data.

3. The 80 x 120 data show reasonable agreement ($\Delta F_M = 0.03$) with the model-scale data except at the two highest 80 x 120 thrust conditions. Contrary to expectations, less power was required with the model-scale than full-scale.

4. CAMRAD II predictions match well with the 80 x 120 data at low thrust. The predictions fall between the flight test results, ovepredicting the 12th Year data (up to $\Delta F_M = 0.02$) and underpredicting the 1st Year data (up to $\Delta F_M = 0.03$).

Forward Flight Data

5. 80 x 120 forward-flight speed sweep and thrust sweep data show smooth trends and are consistent with previously acquired low-speed data. It is anticipated that these data will provide an excellent validation set for analytical development.

6. The 80 x 120 and UH-60A Airloads Program data match well (within $\Delta C_P/\sigma = 0.0002$) at advance ratios above 0.09, but do not match well below this speed ($\Delta C_P/\sigma = 0.0015$).

7. The 80 x 120 and DNW model-scale data match well (within $\Delta C_P/\sigma = 0.0002$) throughout the thrust range for all advance ratios tested. Contrary to expectations, the same power was required with the model-scale as the full-scale data.

8. CAMRAD II shows fair agreement with power, but improvements are needed. The general result is that CAMRAD II overpredicts the required power and that this overprediction increases with increasing lift, shaft angle and advance ratio (up to $\Delta C_P/\sigma = 0.0006$). CAMRAD II shows good agreement with propulsive force. Its calculations with 80 x 120 data correlates within $\Delta C_{XR}/\sigma = 0.001$.

ACKNOWLEDGEMENT

We would like to acknowledge the significant efforts of the UH-60/LRTA test team in the conduct of this test program.

REFERENCES

1. Shinoda, P.M., “Performance Results from a Test on an S-76 Rotor in the NASA Ames 80- by 120-Foot Wind Tunnel,” AIAA Applied Aerodynamics Conference, Monterey, CA, August 1993.

2. Yamakawa, G.M., Bender, G.L., Buckanin, R.M., Robbins, R.D., Bailes, E.E., and Tulloch, J.S., "Production Validation Test Government (PVT-G), Performance Guarantees, UH-60A Black Hawk Helicopter," USAAEFA Project No. 77-23, October 1979.

3. Nagata, J.I., Robbins, R.D., Skinner, G.L., Williams, R.A., and Buckanin, R.M., "Airworthiness and Flight Characteristics Evaluation UH-60A (Black Hawk) Helicopter," USAAEFA Project No. 77-17, September 1981.

4. Williams, R.A., Buckanin, R.M., MacMullin, R., Abbott, W., Miess, J.C., and Skinner, G.L., "UH-60A External Stores Support System Fixed Provision Fairing Drag Determinations," USAAEFA Project No. 82-15-1, May 1984.

5. Marshall, Jr., A.R., MacCullin, R., Lockwood, R.A., Reynolds, T.L., Tavares, E.J., Buckanin, R.M., Skinner, F.L., Herbst, M.K., Cassil, C.F., Sullivan, P.J., and Williams, R.A., "Airworthiness and Flight Characteristics Test of a Sixth Year Production UH-60A," USAAEFA Project No. 83-24, June 1985.

6. Nagata, J.I., Lewis, W.D., Piotrowski, J.L., Losier, P.W., Young, C.J., and Lyle, J.A., "Baseline Performance Verification of the 12th Year Production UH-60A Black Hawk Helicopter," USAAEFA Project No. 87-32, January 1989.

7. Hamade K. S., Kufeld, R. M., "Modal Analysis of UH-60A Instrumented Rotor Blades," NASA TM 4239, November 1990.

8. Kufeld, R. M. and Loschke, P. S., "UH-60A Airloads Program: Status and Plans," AIAA/AHS/ASEE Aircraft Design System and Operations Meeting, Baltimore, MD, September 1991.

9. Cross, J. L., Brilla, J. A., Kufeld, R. M., and Balough, D. L., "Modern Rotor Aerodynamic Limits Survey, Report and Data Survey," NASA TM 4446, October 1993.

10. Kufeld, R. M., Cross, J. L., and Bousman, W. G., "A Survey of Rotor Loads Distribution in Maneuvering Flight," American Helicopter Society Aeromechanics Specialist Conference, San Francisco, CA, January 1994.

11. Kufeld, R. M., Balough, D. L., Cross, J. L., Studebaker, K. L., Jennison, C. D., and Bousman, W. G., "Flight Testing The UH-60A Airloads Aircraft," American Helicopter Society 50th Annual Forum, Washington D.C., May 1994.

12. Kufeld, R. M. and Bousman, W. G., "High Load Conditions Measured On A UH-60A In Maneuvering Flight," American Helicopter Society 51st Annual Forum, Fort Worth, TX, May 1995.

13. Kufeld, R. M. and Bousman, W. G., "UH-60A Helicopter Rotor Airloads Measured in Flight," European Rotorcraft 22nd Forum, Brighton, United Kingdom, September 1996.

14. Kufeld, R. M. and Bousman, W. G., "UH-60A Helicopter Rotor Airloads Measured in Flight," The Aeronautical Journal of the Royal Aeronautical Society, May 1997.

15. Bousman, W. G., "A Qualitative Examination of Dynamic Stall from Flight Test Data," American Helicopter Society 53rd Annual Forum, Virginia Beach, Virginia, April-May 1997.

16. Bousman, W.G., "Power Measurement Errors on a Utility Aircraft," American Helicopter Society Aerodynamics, Acoustics, and Test and Evaluation Technical Specialists Meeting, San Francisco, CA, January 2002.

17. Balch, T.B., "Experimental Study of Main Rotor/Tail Rotor /Airframe Interaction in Hover," Journal of the American Helicopter Society, Vol. 30, (2), April 1985.

18. Lorber, P.F., Stauter, R.C., Pollack, M.J., and Landgrebe, A.J., "A Comprehensive Hover Test of the Airloads and Airflow of an Extensively Instrumented Model Helicopter Rotor; Volume 1 – Rotor Airloads and Performance," USAAVSCOM TR 91-D-16A, October 1991.

19. Lorber, P.F., Stauter, R.C., and Landgrebe, A.J., "A Comprehensive Hover Test of the Airloads and Airflow of an Extensively Instrumented Model Helicopter Rotor," American Helicopter Society 45th Annual Forum, Boston, MA, May 1989.

20. Lorber, P.F., "Pressure-Instrumented Model UH-60A Black Hawk Rotor Test at DNW; Volume 1 Description of Experiment," United Technologies Research Center R91-153577-1, February 1991.

21. Lorber, P.F., "Pressure-Instrumented Model UH-60A Black Hawk Rotor Test at DNW; Volume 2 Contour Plots and Tabulated Data," United Technologies Research Center R91-153577-2, February 1991.

22. Lorber, P.F., "Aerodynamic Results of a Pressure-Instrumented Model Rotor Test at the DNW," Journal of the American Helicopter Society, Vol. 36, (4), October 1991.

23. Norman, T.R., Shinoda, P.M., Kitaplioglu, C., Jacklin, S.A., and Sheikman, A., "Low-Speed Wind Tunnel Investigation of a Full-Scale UH-60 Rotor System," American Helicopter Society 58th Annual Forum, Montreal, Canada, June 2002.

24. Van Aken, J. M., Shinoda, P. M., and Haddad, F., "Development of a Calibration Rig for a Large Multi-Component Rotor Balance," 46th International Instrumentation Symposium of the Instrument Society of America, Bellevue, WA, May 2000.

25. Heyson, H.H., "Use of Superposition on Digital Computers to Obtain Wind Tunnel Interference Factors for Arbitrary Configurations, with Particular Reference to V/STOL Models," NASA TR R-302, February 1969.

26. Yeo, H., Bousman,W.G., and Johnson, W., "Performance Analysis of a Utility Helicopter with Standard and Advanced Rotors," American Helicopter Society Aerodynamics, Acoustics, and Test and Evaluation Technical Specialists Meeting, San Francisco, CA, January 2002.

27. Johnson, W., "Rotorcraft Aerodynamics Model for a Comprehensive Analysis," American Helicopter Society 54th Annual Forum, Washington, D.C., May 1998.

28. Bousman, W.G., "Out-of-Ground-Effect Hover Performance of the UH-60A," UH-60 Airloads Program Occasional Note 2001-01, February 2001, http://rotorcraft.arc.nasa.gov/research/pdfs/2001-01.pdf.

29. Keys, C.N., McVeigh, M.A., Dadone, L., and McHugh, F.J. "Considerations in the Estimation of Full-Scale Rotor Performance from Model Rotor Test Data," American Helicopter Society 39th Annual Forum, St. Louis, MO., May 1983.

Table 1. Main Rotor Parameters

Parameter	Value
Number of Blades	4
Radius	26.83 ft.
Chord	20.76 / 20.965 in.
Thickness, % chord	9.5 / 9.4
Rotor Disk Area	2261.5 ft^2
Rotor Blade Area	186.9 ft^2
Solidity Ratio	.0826
Blade tip sweep, aft	20 deg
Airfoils	SC1095/ SC1094 R8
Nominal Rotor Speed	258 rpm
Nominal Tip Speed	725 ft/sec

Table 2. Rotor Balance Capabilities

Parameter	Capacity Max.
Thrust	52,000 lbs
Hub Force (Combined Axial/ Side Force)	15,000 lbs
Hub Moment (Combined Pitch/ Roll Moment)	50,000 ft-lbs
Torque	165,000 ft-lbs

Table 3. LRTA Balance Accuracy

Parameter	Maximum Cal. Load	Estimated Uncertainty	
		Value	%
Normal Force	30,000 lb	60 lb	0.20
Axial Force	15,000 lb	20 lb	0.13
Side Force	15,000 lb	20 lb	0.13
Pitch Moment	83,000 ft-lb	100 ft-lb	0.12
Roll Moment	83,000 ft-lb	200 ft-lb	0.24

Table 4. Hover Test Matrix

Shaft Angles, α_S	-7.5°, 0°, 7.5°, -15°
C_T/σ	0.02 – 0.07
Tip Mach No., M_{TIP}	0.650

Table 5. Speed Sweep Test Matrix

α_S	C_T/σ	μ
0°	0.06, 0.08,0.09	0 to 0.190
-5°	0.09	0 to 0.190

M_{TIP} =0.650

Table 6. Thrust Sweep Test Matrix

Advance Ratio μ	Rotor Shaft Angle-of-Attack α_s	Approx. C_T/σ Range
0.050	-10°, -5°, 0°, 5°	.02 - .11
0.100	-10°, -5°, 0°, 5°, 10°	.02 - .11
0.150	-10°, -5°, 0°, 5°	.02 - .11
0.175	-10°, -5° ,0°, 5°, 7.5°	.02 - .11
0.190	-10°, -5° ,0°, 5°	.02 - .11

M_{TIP} =0.650

Fig. 1. UH-60 Rotor System installed on Large Rotor Test Apparatus in the Ames 80- by 120-Foot Wind Tunnel.

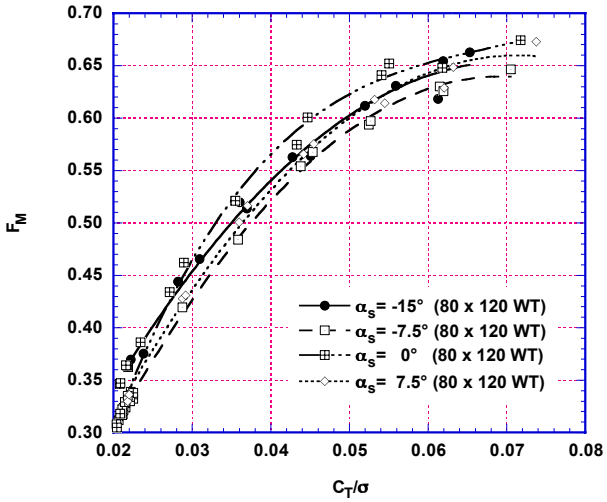

Fig. 2. Effect of shaft angle on rotor figure of merit, M_{TIP} = 0.650.

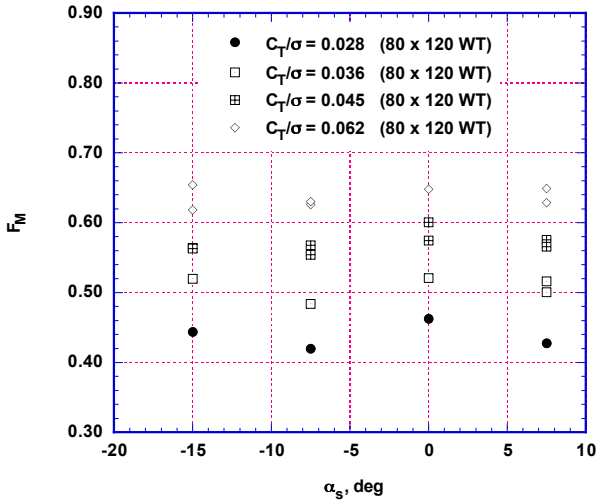

Fig. 3. Effect of rotor shaft angle sweep on figure of merit at C_T/σ = 0.028, 0.036, 0.045, 0.062, M_{TIP} = 0.650.

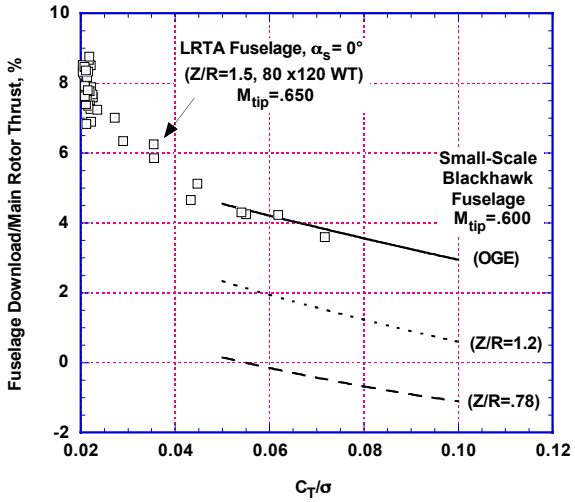

Fig. 4. Comparison of LRTA fuselage and small-scale UH-60 aircraft fuselage download in percentage of rotor thrust, M_{TIP} = 0.650 and M_{TIP}= 0.600, respectively.

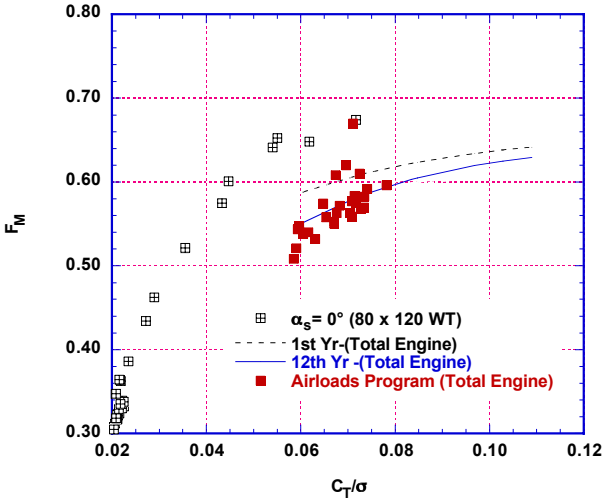

Fig. 6. UH-60 rotor hover figure of merit comparison with three helicopter aircraft experiments (no corrections).

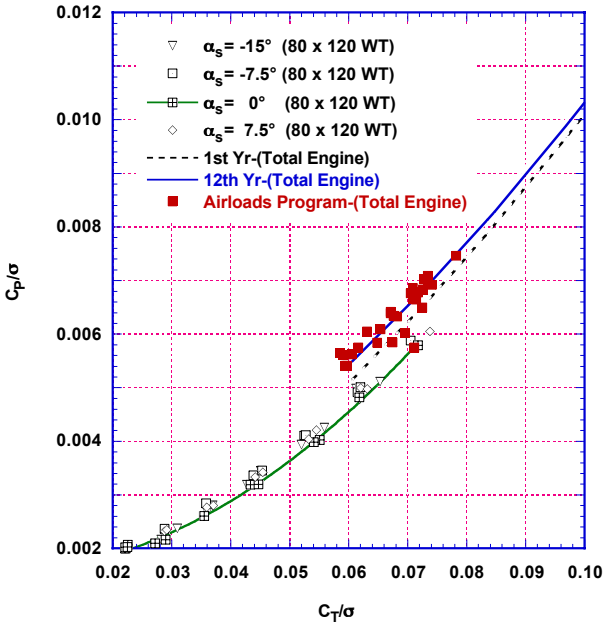

Fig. 5. UH-60 rotor hover power comparison with three helicopter aircraft experiments (no corrections).

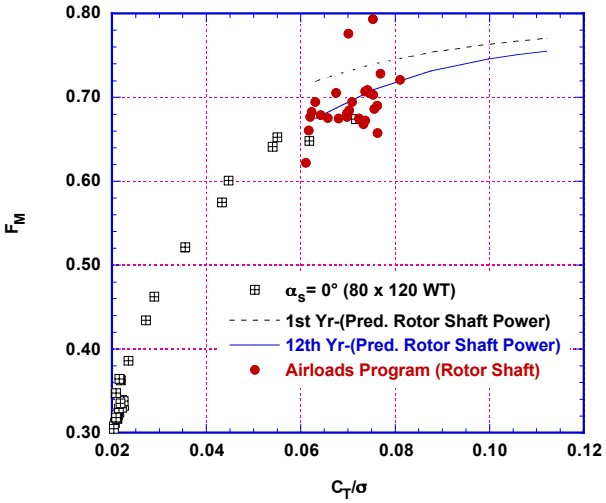

Fig. 7. UH-60 rotor hover figure of merit comparison with three helicopter aircraft experiments (with corrections).

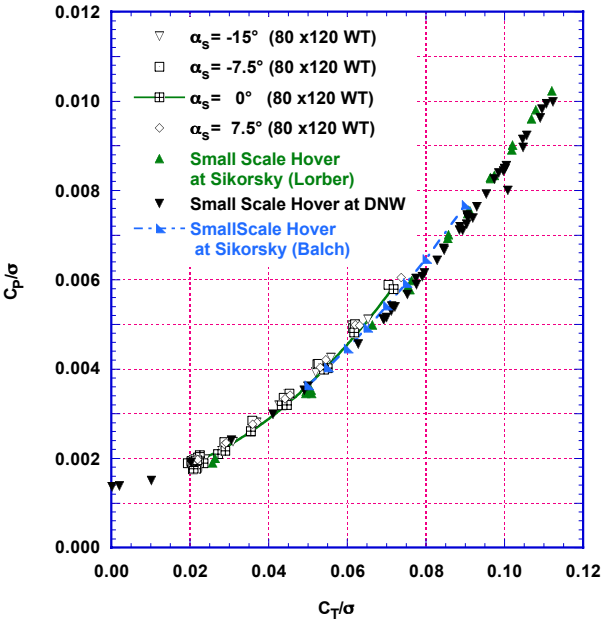

Fig. 8. UH-60 rotor hover power comparison with three model-scale experiments (no scale-effect corrections).

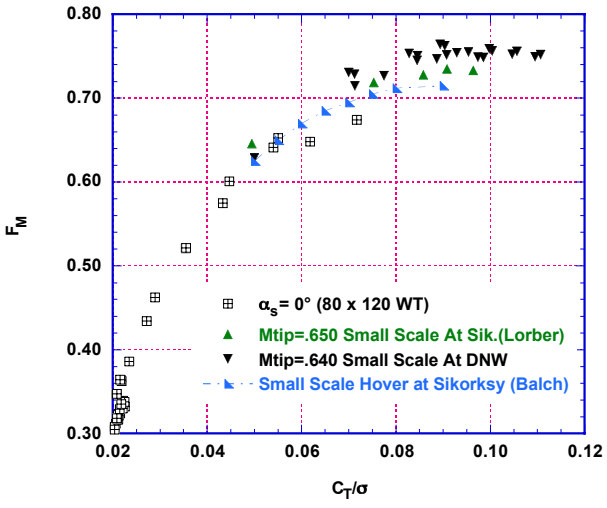

Fig. 9. UH-60 rotor hover figure of merit comparison with three model-scale experiments (no scale-effect corrections).

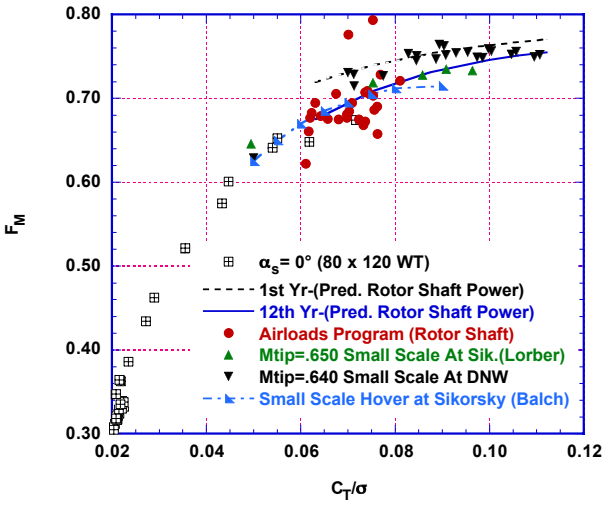

Fig. 10. UH-60 rotor hover figure of merit comparison with three helicopter aircraft experiments (with corrections) and three model-scale experiments (no scale-effect corrections).

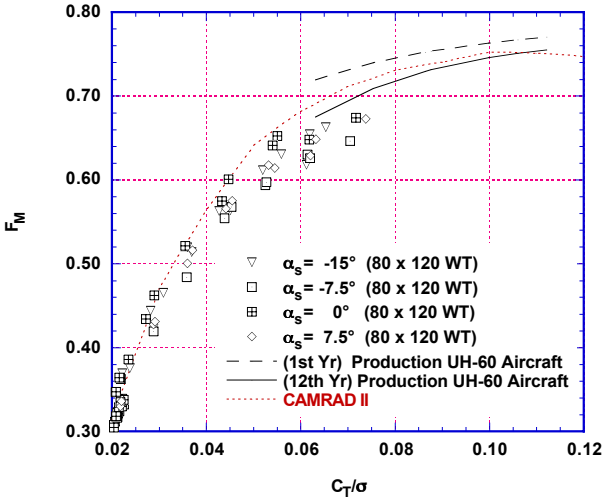

Fig. 11. UH-60 rotor hover figure of merit comparison with three helicopter aircraft experiments and predictions.

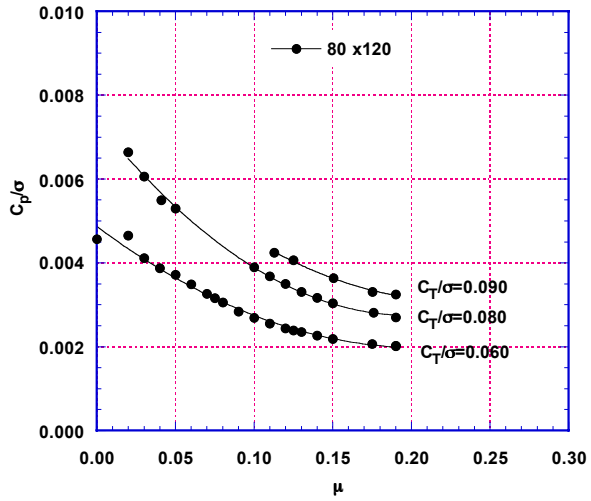

Fig. 12. Measured 80 x 120 rotor power vs. advance ratio, α_s = 0 deg, C_T/σ = 0.060, 0.080, 0.090, M_{TIP} = 0.650.

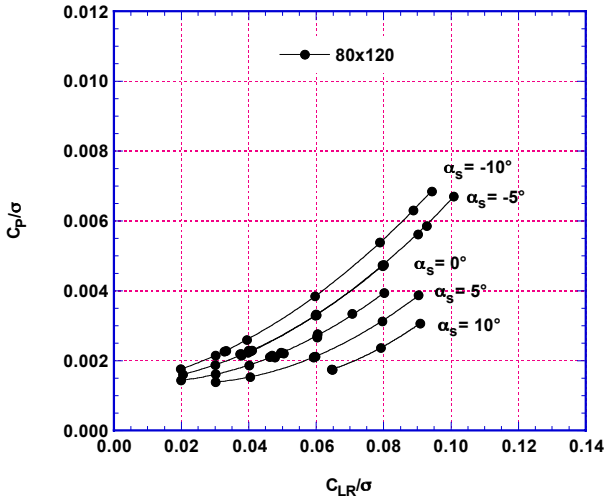

Fig. 14. Measured 80 x 120 rotor power vs. rotor lift for various rotor shaft angles at an advance ratio of 0.100, M_{TIP} = 0.650.

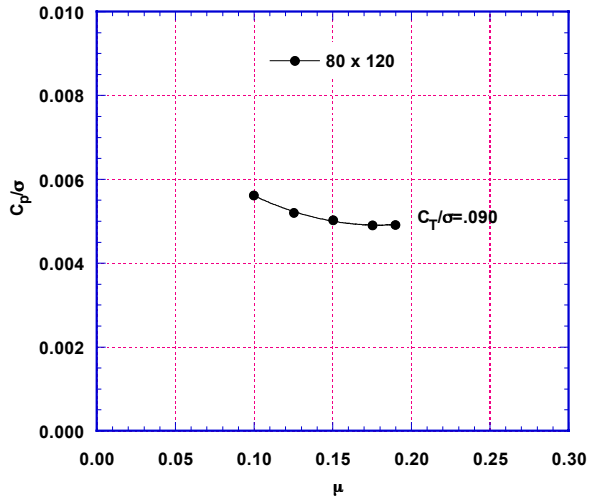

Fig. 13. Measured 80 x 120 rotor power vs. advance ratio, α_s = -5 deg, C_T/σ = 0.090, M_{TIP} = 0.650.

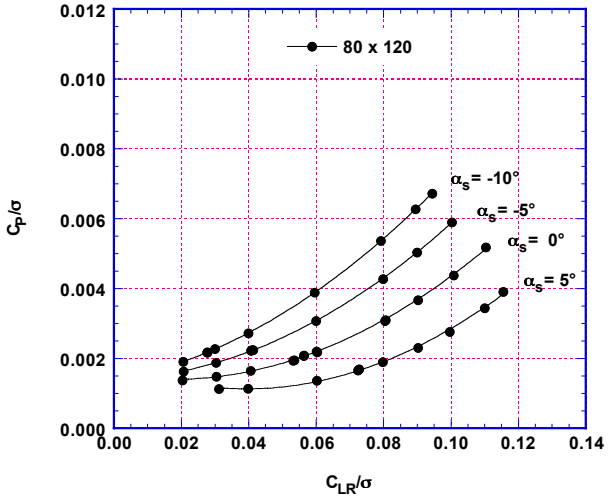

Fig. 15. Measured 80 x 120 rotor power vs. rotor lift for various rotor shaft angles at an advance ratio of 0.150, M_{TIP} = 0.650.

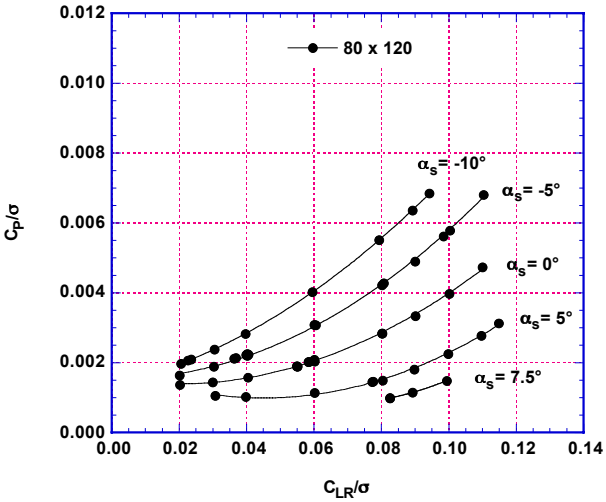

Fig. 16. Measured 80 x 120 rotor power vs. rotor lift for various rotor shaft angles at an advance ratio of 0.175, $M_{TIP} = 0.650$.

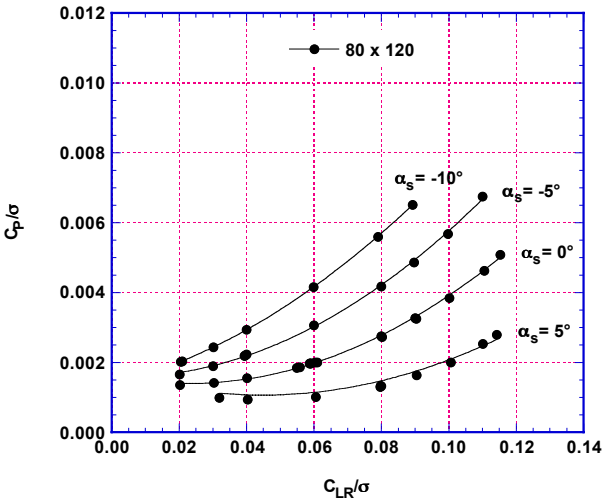

Fig. 17. Measured 80 x 120 rotor power vs. rotor lift for various rotor shaft angles at an advance ratio of 0.190, $M_{TIP} = 0.650$.

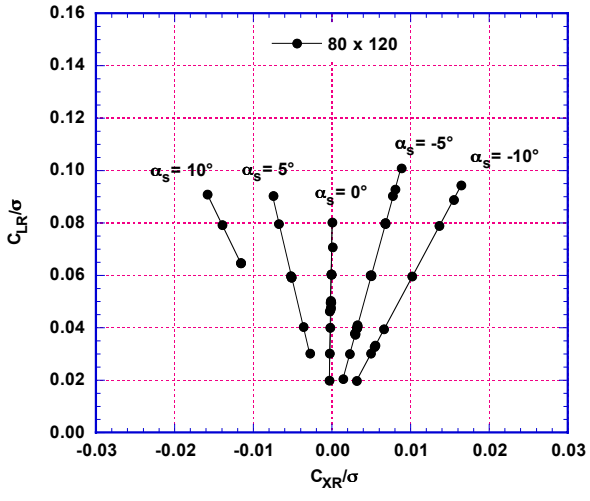

Fig. 18. Measured 80 x 120 rotor propulsive force vs. rotor lift for various rotor shaft angles at an advance ratio of 0.100, $M_{TIP} = 0.650$.

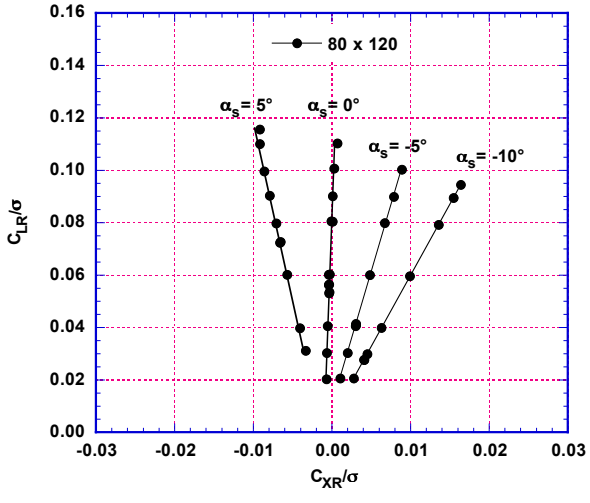

Fig. 19. Measured 80 x 120 rotor propulsive force vs. rotor lift for various rotor shaft angles at an advance ratio of 0.150, $M_{TIP} = 0.650$.

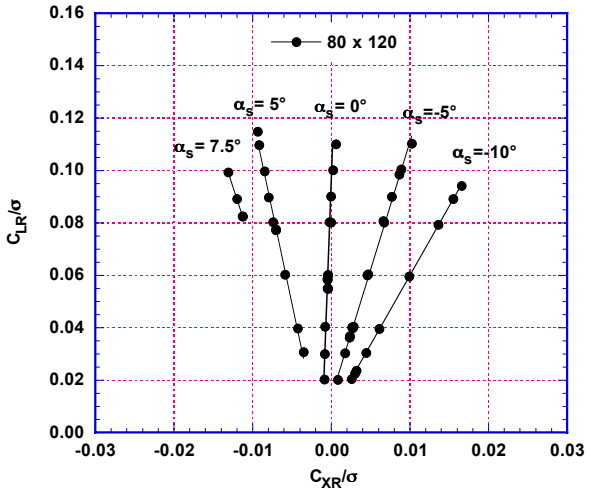

Fig. 20. Measured 80 x 120 rotor propulsive force vs. rotor lift for various rotor shaft angles at an advance ratio of 0.175, $M_{TIP} = 0.650$.

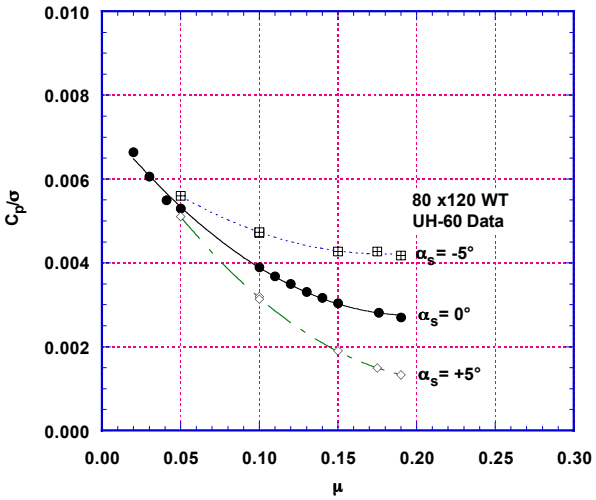

Fig. 22. Measured 80 x 120 rotor power vs. advance ratio, with curve fits, $C_{LR}/\sigma = 0.080$, $M_{TIP} = 0.650$.

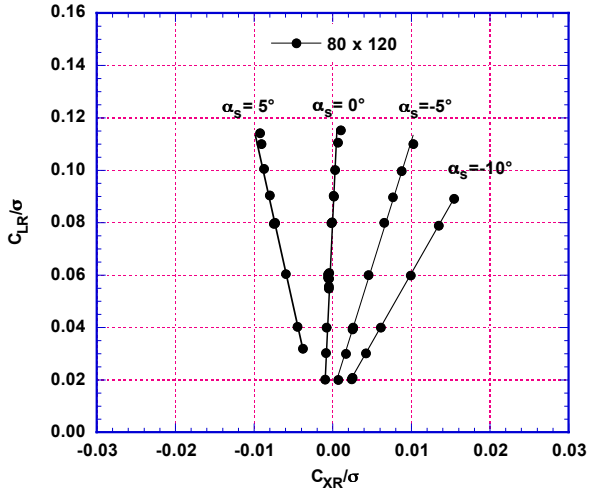

Fig. 21. Measured 80 x 120 rotor propulsive force vs. rotor lift for various rotor shaft angles at an advance ratio of 0.190, $M_{TIP} = 0.650$.

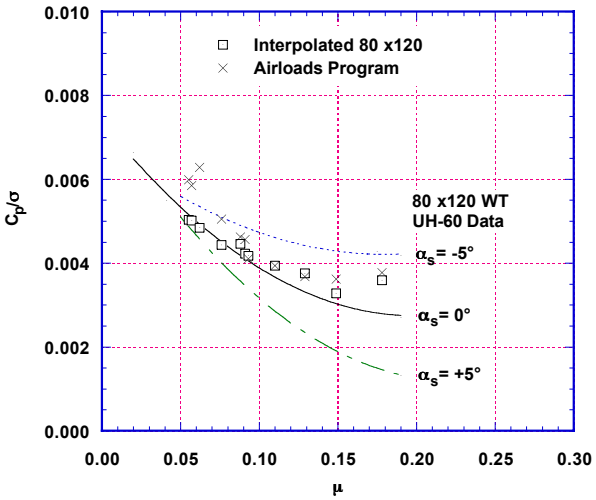

Fig. 23. Comparison of Airloads Program with 80 x 120 measured rotor power, C_{LR}/σ and $C_W/\sigma = 0.080$, $M_{TIP} = 0.650$.

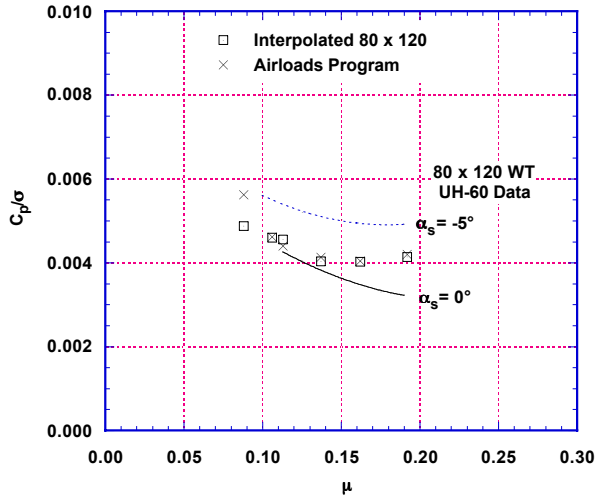

Fig. 24. Comparison of Airloads Program with 80 x 120 measured rotor power, C_{LR}/σ and $C_W/\sigma = 0.090$, $M_{TIP} = 0.650$.

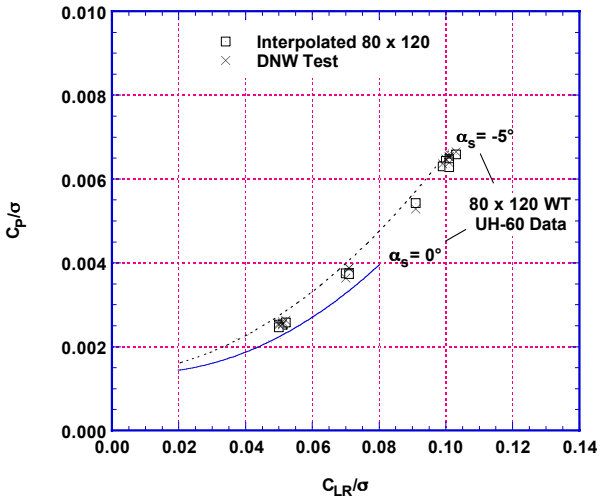

Fig. 26. Comparison of DNW with 80 x 120 measured rotor power for an advance ratio of 0.100, $M_{TIP} = 0.650$ (80 x120), 0.636 (DNW).

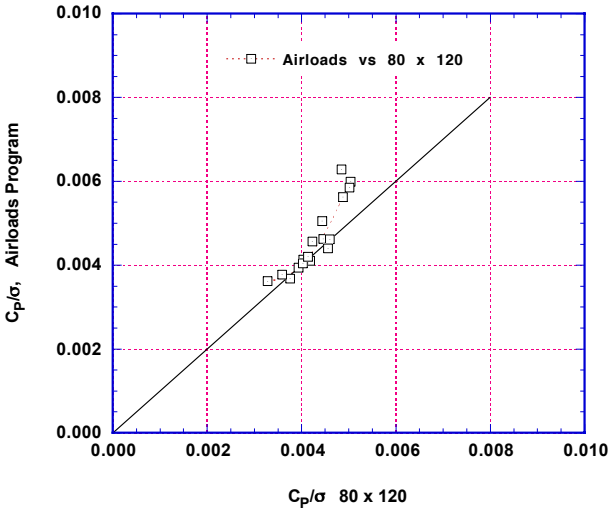

Fig. 25. Airloads Program rotor power vs. 80 x 120 rotor power at all advance ratios, thrust condition, and tip-plane-angles.

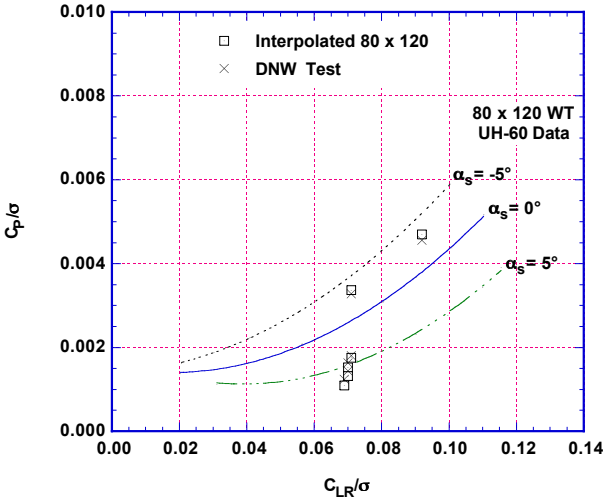

Fig. 27. Comparison of DNW with 80 x 120 measured rotor power for an advance ratio of 0.150, $M_{TIP} = 0.650$ (80 x120), 0.636 (DNW).

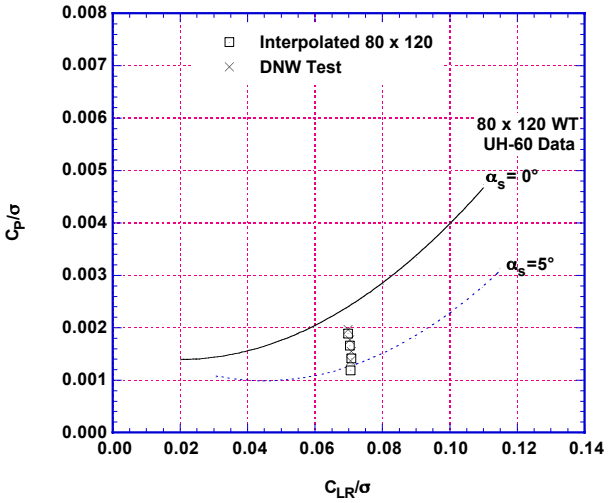

Fig. 28. Comparison of DNW with 80 x 120 measured rotor power for an advance ratio of 0.175, M_{TIP} = 0.650 (80 x120), 0.636 (DNW).

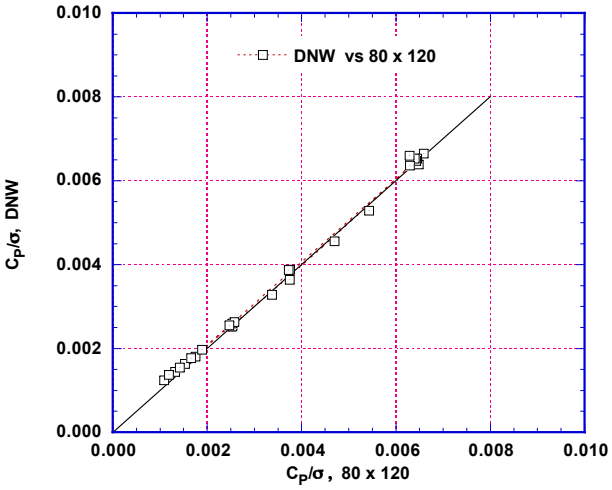

Fig. 29. DNW rotor power vs. 80 x 120 rotor power at all advance ratios, thrust condition, and tip-plane-angles.

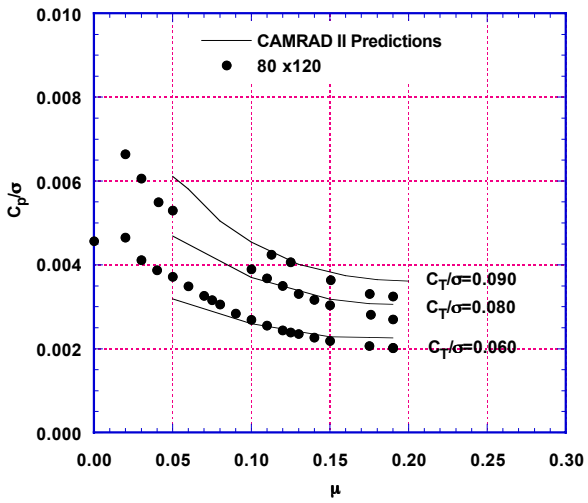

Fig. 30. Measured and calculated rotor power vs. advance ratio for various thrust conditions, α_s = 0 deg, M_{TIP} = 0.650.

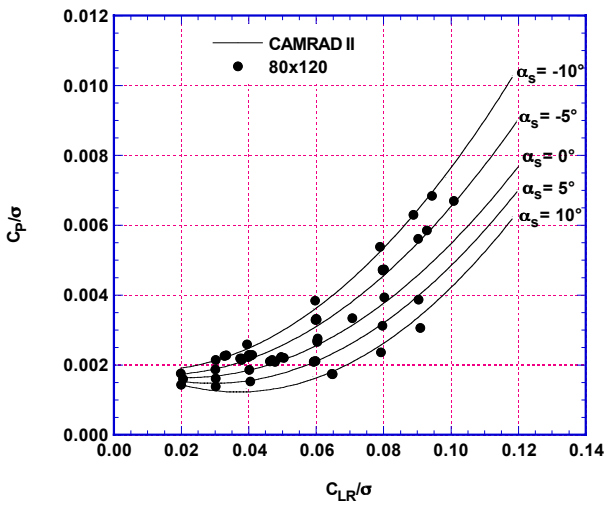

Fig. 31. Measured and calculated rotor power vs. rotor lift for various rotor shaft angles at an advance ratio of 0.100, M_{TIP} = 0.650.

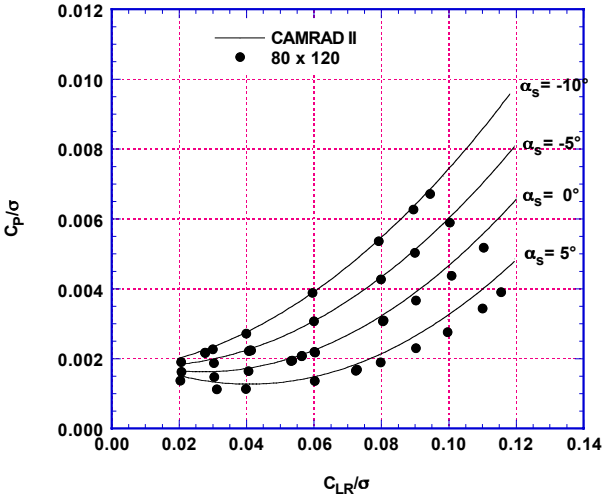

Fig. 32. Measured and calculated rotor power vs. rotor lift for various rotor shaft angles at an advance ratio of 0.150, $M_{TIP} = 0.650$.

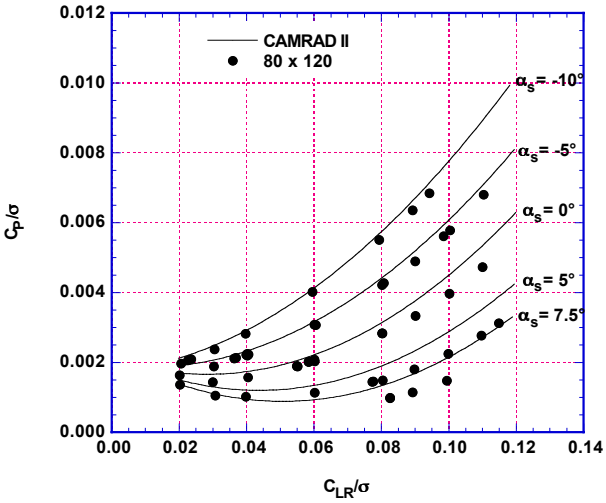

Fig. 33. Measured and calculated rotor power vs. rotor lift for various rotor shaft angles at an advance ratio of 0.175, $M_{TIP} = 0.650$.

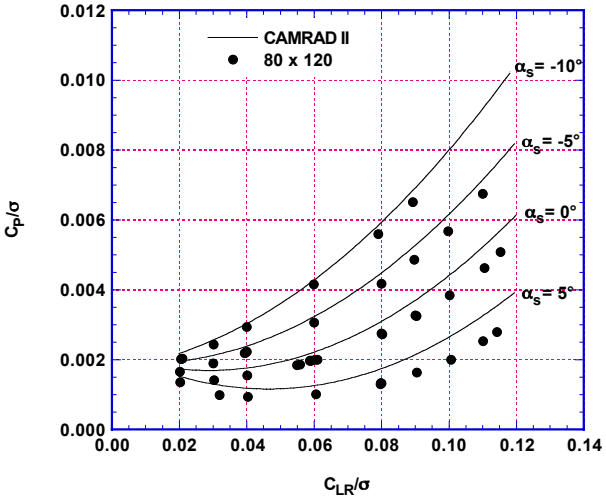

Fig. 34. Measured and calculated rotor power vs. rotor lift for various rotor shaft angles at an advance ratio of 0.190, $M_{TIP} = 0.650$.

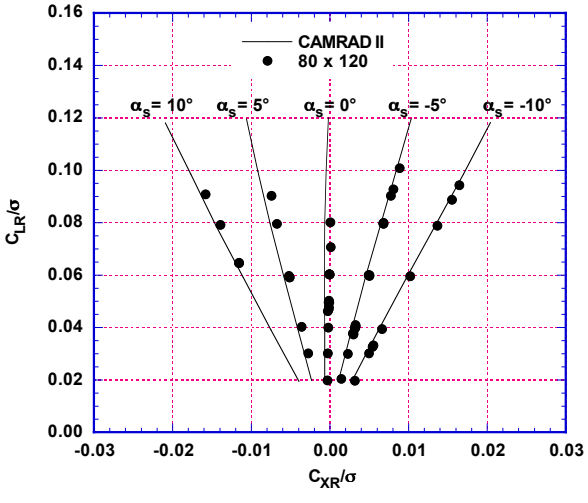

Fig. 35. Measured and calculated rotor propulsive force vs. rotor lift for various rotor shaft angles at an advance ratio of 0.100, $M_{TIP} = 0.650$.